Pharm Res (2015) 32:1264–1278
DOI 10.1007/s11095-014-1531-z

RESEARCH PAPER

Targeting, Endocytosis, and Lysosomal Delivery of Active Enzymes to Model Human Neurons by ICAM-1-Targeted Nanocarriers

Janet Hsu • Janet Hoenicka • Silvia Muro

Received: 24 June 2014 / Accepted: 24 September 2014 / Published online: 16 October 2014

ABSTRACT

Purpose Delivery of therapeutics to neurons is paramount to treat neurological conditions, including many lysosomal storage disorders. However, key aspects of drug-carrier behavior in neurons are relatively unknown: the occurrence of non-canonical endocytic pathways (present in other cells); whether carriers that traverse the blood–brain barrier are, contrarily, retained within neurons; if neuron-surface receptors are accessible to bulky carriers compared to small ligands; or if there are differences regarding neuronal compartments (neuron body vs. neurites) pertaining said parameters. We have explored these questions using model polymer nanocarriers targeting intercellular adhesion molecule-1 (ICAM-1).

Methods Differentiated human neuroblastoma cells were incubated with anti-ICAM-coated polystyrene nanocarriers and analyzed by fluorescence microscopy.

Results ICAM-1 expression and nanocarrier binding was enhanced in altered (TNFα) vs. control conditions. While small ICAM-1 ligands (anti-ICAM) preferentially accessed the cell body, anti-ICAM nanocarriers bound with faster kinetics to neurites, yet reached similar saturation over time. Anti-ICAM nanocarriers were also endocytosed with faster kinetics and lower saturation levels in neurites. Non-classical cell adhesion molecule (CAM) endocytosis ruled uptake, and neurite-to-cell body transport was inferred. Nanocarriers trafficked to lysosomes, delivering active enzymes (dextranase) with substrate reduction in a lysosomal-storage disease model.

Conclusion ICAM-1-targeting holds potential for intracellular delivery of therapeutics to neurons.

KEY WORDS CAM-mediated endocytosis · ICAM-1-targeted nanocarriers · Lysosomal transport · neuroblastoma cells · neuronal body vs. neurites

ABBREVIATIONS

BBB	Blood–brain barrier
Bmax	Maximal binding
FBS	Fetal bovine serum
FITC	Fluorescein isothiocyanate
ICAM-1	Intercellular adhesion molecule-1
IgG	Immunoglobulin G
Imax	Maximal internalization
LSD	Lysosomal storage disorder
MDC	Monodansylcadaverine
NC	Nanocarrier
PBS	Phosphate buffer saline
PDI	Polydispersity index
Tmax	Maximal transport to lysosomes.

INTRODUCTION

Neurons represent a key target for the treatment of a myriad of diseases where neuropathy and/or neurodegeneration affect the central or peripheral nervous system [1]. These include (among many others) cerebral, cerebellar, spinal, and peripheral degenerations affecting behavioral, cognitive and/

J. Hsu • S. Muro
Fischell Department of Bioengineering, University of Maryland College Park, Maryland 20742, USA

J. Hoenicka
Program in Rare and Genetic Diseases & IBV/CSIC Associated Unit Centro de Investigación Príncipe Felipe Valencia, Spain

J. Hoenicka
Centro de Investigación Biomédica en Red de Salud Mental (CIBERSAM) ISCIII Valencia, Spain

S. Muro (✉)
Institute for Bioscience and Biotechnology Research, University of Maryland College Park, Maryland 20742, USA
e-mail: muro@umd.edu

or motor skills [1]. Such is the case for Alzheimer's disease and other forms of dementia, Parkinson's disease, ataxias, and other conditions affecting motor control, multiple sclerosis and other demyelinating disorders, complex behavioral and addiction traits, etc. [1]. Therefore, drug delivery to the brain and the neuro-muscular system has become a focal area of investigation and development [2].

Within this arena, transport of pharmaceuticals across the interface that separates the bloodstream from the brain tissue, the blood–brain barrier (BBB), has gained much interest as it represents a paramount obstacle to effective drug delivery into the central nervous system (CNS). Strategies aimed at bypassing this barrier involve local administration into the CNS [2], administration through the intranasal route [3], the use of exosomes [4], enhancement of paracellular permeability between adjacent endothelial cells in the BBB [5], and induction of transcellular transport via vesicular transcytosis across the cell body of these cells [6]. These approaches hold considerable promise to advance treatment of neurological conditions by improving delivery of therapeutic molecules into the CNS. However, even after crossing the BBB, a pharmaceutical agent must still interact with its therapeutic target within the brain. As for other tissues, most therapeutic targets are located intracellularly, hence strategies to improve the interaction of drugs with neurons and their transport to intracellular compartments in these cells are of key importance.

Drug delivery systems in the submicrometer-size range (also called drug nanocarriers) have the capability to improve this aspect. These platforms can increase the therapeutic potential of pharmaceutical agents by enhancing drug solubility, circulation, degradation, and release [7]. Functionalization of such drug carriers with affinity moieties (antibodies, peptides, aptamers, etc.) that recognize cell-surface molecules involved in endocytic transport offers the opportunity to address treatments into target cells [8]. Although much knowledge has already been gained from studying receptor binding, endocytosis, and intracellular transport of drug carriers in different cells types, the behavior of these systems with regard to neurons is still relatively scarce. Most studies of drug delivery to neurons have involved carriers that are not targeted to cell-surface receptors, including liposomes, gene delivery vectors, DNA-based complexes, and polymer nanocarriers, among others [9–11], while examples of targeted systems refer to conjugates where a therapeutic agent is linked to an affinity moiety, rather than a particulate drug carrier [12–14]. A few works focusing on transport of targeted drug carriers in neurons have revealed that targeting synapses can trigger synaptic vesicular uptake and retrograde transport toward the cell body, which offers promise for intra-neuronal drug delivery [15].

However, many aspects key to developing such technologies remain obscure. For instance, it is unknown whether receptors targeted to facilitate carrier transport across the BBB have a similar or distinct ability to induce transport within neurons, whether targeted carriers designed to traverse cells of the BBB can be retained efficiently within intra-neuronal compartments, whether amenable receptors for endocytosis into neurons are similarly accessible and effective for small ligands vs. bulkier drug carriers, etc. In addition, little is known about how these events are affected with regard to different regions of neurons, e.g., the cell body vs. cellular processes (neurites), which categorically differ from most other cells with much less distinct morphological (and functional) areas. Finally, although receptors of classical endocytic pathways (most commonly, clathrin- and caveolae-mediated endocytosis) have been explored for neuronal uptake [12, 13, 16, 17], the occurrence and, hence, utility of alternative clathrin- and caveolae-independent uptake mechanisms observed in other cells [8] is largely unknown for neurons, especially for drug delivery.

As a relevant example to gain insight into these aspects, this study focused on carrier targeting to intercellular adhesion molecule 1 (ICAM-1). ICAM-1 is a cell-surface molecule involved in inflammation [18] (a hallmark underlining most diseases) and expressed on many cell types, including those relevant to the BBB (endothelial cells, pericytes, and astrocytes) and neurons, among others [18, 19]. The basal level of ICAM-1 expression is relatively low, yet it is upregulated in most pathological states [18, 19], thus facilitating targeting to diseased sites [19, 20]. ICAM-1 is a co-receptor for β_2 integrins on activated leukocytes [18]; hence, its natural ligand is a large, multivalent "object", in contrast to canonical receptors of small molecular ligands. Accordingly, recent studies suggest that endothelial endocytosis of nanoparticles via ICAM-1 is more efficient compared to that of nanoparticles targeted to receptors of smaller ligands (e.g., the transferrin receptor, the mannose-6-phosphate receptor [21, 22]), while the opposite result was found when using targeting antibodies in the absence of carriers [21, 23]. Uptake of drug carriers via ICAM-1 is efficient under a wide range of carrier sizes (including the micrometer range) both in cell culture and *in vivo* [22–24]. This is regulated by cell adhesion molecule- (CAM)-mediated endocytosis, a pathway that differs from clathrin- and caveolar-mediated endocytosis [24, 25]. Importantly, we recently reported that targeting model polymer nanocarriers to ICAM-1 can induce transcytosis in models of cellular barriers, including gastrointestinal epithelial monolayers [26] and endothelial-subendothelial bilayers mimicking the BBB [19]. Radiotracing of the antibody coat on these carriers showed that this targeting moiety is still present in the fraction of carrier transported across both linings [19]. Yet, in cells that do not form barriers, ICAM-1-targeted carriers are able to deliver therapeutics into cells, including lysosomes [19, 23] and other intracellular destinations when carriers are designed to escape these compartments [27]. Therefore, ICAM-1

targeting meets the requirements of a receptor suitable to explore the questions posed above.

In addition, ICAM-1 represents a relevant target for drug delivery to cope with certain neurological conditions. This is the case for many lysosomal storage disorders (LSDs), a group of 40–50 diseases due to genetic deficiencies affecting lysosomal enzymes [6]. This causes aberrant accumulation of undegraded metabolites within lysosomes throughout the body, leading to fatal dysfunction of peripheral organs and also the CNS [6]. Enzyme replacement therapies aimed to treat these diseases require broad delivery throughout the body, including transport across the BBB and into neurons [6]. Our previous studies have shown that ICAM-1-targeted nanocarriers greatly enhance biodistribution of lysosomal enzymes to all organs in the body (including the brain) in mouse models, with effective delivery to lysosomes within cells [20, 21, 23]. Yet, lysosomal delivery of enzymes via ICAM-1 has never been tested in neurons. In this study, we have examined binding, endocytosis, lysosomal transport, and effects of enzyme delivery by ICAM-1-targeted nanocarriers in model human neurons under both control and altered conditions, and have additionally focused on how these parameters are influenced with regard to different neuronal compartments, namely the neuronal body vs. neurites.

MATERIALS AND METHODS

Antibodies and Reagents

Monoclonal mouse anti-human ICAM-1 (anti-ICAM) was clone R6.5 (American Type Culture Collection; Manassas, VA). Non-specific mouse IgG and secondary goat anti-mouse IgG were from Jackson Immunoresearch (West Grove, PA). Dextranase (Dxase) from *Penicillium janthinellum* was from Sigma Aldrich (St. Louis, MO). Fluoresbrite® polystyrene latex particles were from Polysciences (Warrington, PA). ^{125}Iodine (^{125}I) and Iodogen pre-coated tubes were purchased from PerkinElmer (Waltham, MA) and Thermo Fisher Scientific (Waltham, MA), respectively. Cell culture media and supplements were from Cellgro (Manassas, VA), Gibco BRL (Grand Island, NY), or Sigma Aldrich (St. Louis, MO). Unless otherwise noted, all other reagents were from Sigma Aldrich (St. Louis, MO).

Preparation of ICAM-1-Targeted Nanocarriers

Model polymer nanocarriers (NCs) were prepared by coating 100-nm diameter Fluoresbrite®-polystyrene particles (~10^{13} particles/mL) by surface adsorption for 1 h at room temperature with ~5 μM unlabeled or ^{125}I-labeled anti-ICAM (anti-ICAM NCs) or control IgG (IgG NCs), or a mix of anti-ICAM and Dxase (2:1 molar ratio; anti-ICAM/Dxase NCs), as described [19]. Non-coated antibody was removed by centrifugation at 13,800 g for 3 min. Coated particles were resuspended at ~7×10^{11} NCs/mL in phosphate buffered saline (PBS) containing 1% bovine serum albumin, followed by low power sonication to dissolve aggregates. Size was measured by particle tracking (Nanosight LM10, Malvern Instruments; Westborough, MA), while polydispersity index (PDI) and ζ-potential were measured by dynamic light scattering and electrophoretic mobility, respectively (Zetasizer Nano-ZS90, Malvern Instruments; Westborough, MA). The antibody or enzyme coat density were assessed by measuring the ^{125}I content in a gamma counter (2470 Wizard2, Perkin Elmer; Waltham, MA) to calculate the number of antibody or enzyme molecules per particle, based on the known particle concentration (see above) and ^{125}I-antibody or ^{125}I-enzyme specific activity (cpm/mass), as described [19].

Cell Cultures

Human neuroblastoma SH-SY5Y cells (American Type Culture Collection; Manassas, VA) were seeded on Matrigel® (BD Biosciences; Franklin Lakes, NJ) and cultured in 37°C, 5% CO_2 and 95% relative humidity. Cells were first propagated in RPMI medium supplemented with 10% fetal bovine serum (FBS), 2 mM glutamine, and 1 mM pyruvate. For experiments, cells were differentiated into neuron-like cells (herein referred to as neurons), as described [28]. Briefly, cells were seeded at 7.5×10^3 cells/cm^2 and grown in DMEM supplemented with 5% FBS and 10 μM retinoic acid for 5 days, exchanging old medium with fresh medium every other day. Then, cells were cultured for 5 days in Neurobasal medium supplemented with 1% B-27, 50 μg/mL gentamicin, 2 mM GlutaMaxI, 2 mM dibutyryl-cyclic AMP, 20 mM potassium chloride, 50 ng/mL recombinant human brain-derived neurotrophic factor, 100 U/mL penicillin, and 100 μg/mL streptomycin, also exchanging the cell medium every other day [28]. Where indicated, cells were treated with 10 ng/mL tumor necrosis factor α (TNFα) for 16 h to activate ICAM-1 expression as in many pathological conditions involving inflammation.

ICAM-1 Expression

The expression of ICAM-1 on the surface of control vs. TNFα-activated cells was assessed by immunostaining and fluorescence microscopy, as described [19]. Cells were fixed with cold 2% paraformaldehyde for 15 min and then incubated with ~55 pM anti-ICAM or non-specific IgG for 1 h at room temperature. Primary antibody was then removed, followed by incubation for 30 min at room temperature with ~25 pM FITC-labeled secondary antibody. Images were analyzed by fluorescence microscopy using an Olympus IX81 microscope (Olympus, Inc., Center Valley, PA) with a

40× objective and DAPI, FITC, and Texas-Red filters (1160A-OMF, 3540B-OMF, 4040B-OMF; Semrock Inc.; Rochester, NY). Pictures were taken with an ORCA-ER camera (Hamamatsu; Bridgewater, New Jersey) using SlideBook 4.2 software (Intelligent Imaging Innovations; Denver, Colorado) and analyzed with Image-Pro 6.3 (Media Cybernetics; Bethesda, Maryland). Background fluorescence in each microscopy image was subtracted. Specific ICAM-1 expression was compared to non-specific IgG.

Binding and Internalization of ICAM-1-Targeted Nanocarriers

Control vs. TNFα-activated cells were incubated at 37°C with green Fluoresbrite® anti-ICAM NCs for 1, 3, or 5 h. Incubations were done in the absence vs. presence of inhibitors of endocytic pathways, including 3 mM amiloride to inhibit CAM-mediated endocytosis, 1 μg/mL filipin to block caveolae-mediated pathways, or 50 μM monodansylcadaverine (MDC) to inhibit clathrin-mediated uptake, as previously reported [20, 25]. After this time, the cell medium containing non-bound carriers was removed, and cells were washed and fixed with paraformaldehyde. Samples were then incubated with a Texas-Red-labeled secondary antibody to stain anti-ICAM on the coat of carriers bound to the surface of cells (non-internalized) and ~14 μM 4′,6-diamidino-2-phenylindole (DAPI) to stain cell nuclei. Hence, cell surface-bound carriers appear yellow (green+red) when visualized by fluorescence microscopy, while internalized carriers (not accessible to this secondary staining) fluoresce only under the green channel. The total number of anti-ICAM NCs associated per cell, bound to the cell surface, and internalized within cells were quantified as described previously [20, 25]. This is possible since the Fluoresbrite® signal of carriers is not sensitive to potential different pH of intracellular compartments. We used an algorithm that normalizes the area of specific fluorescence (over a threshold background) to the number of pixels that theoretically correspond to the size of a single particle, viewed under the magnification used to take images. The percentage (rate) of internalization was calculated as the fraction of internalized carriers compared to the total number of carriers associated per cell. These parameters were also analyzed differentially for the cell body vs. neurites and, where indicated, normalized to the apparent 2D area occupied by these subcellular regions.

Potential Transport of Anti-ICAM NCs Between Cell Compartments

TNFα-activated cells were incubated for 1 h at 37°C with green Fluoresbrite® anti-ICAM NCs, followed by removing carriers from the cell medium to avoid subsequent binding and uptake that may confound tracking of carriers already associated to cells. Cells were either fixed at this time point or incubated in control medium for 2 or 4 additional hours to track changes in the pattern of cell-associated carriers over time (total incubation time was 1, 3, or 5 h). Samples were imaged by fluorescence microscopy as described above and the fraction (percentage) of anti-ICAM NCs located in neurites vs. the cell body was quantified over time.

Lysosomal Trafficking of ICAM-1-Targeted Nanocarriers

Lysosomes of TNFα-activated cells were labeled, as previously described [29], by pre-incubating cells for 45 min at 37°C with 1 mg/ml Texas-Red dextran (10 kDa), to allow endocytosis of this fluid-phase marker. Cells were then washed and incubated in control medium for 45 min to ensure dextran accumulation in the endo-lysosomal system. Since mammalian cells cannot degrade this polysaccharide, dextran remains stable within lysosomes, permitting their visualization. We have previously verified the colocalization of dextran and the lysosomal marker Lamp-1 in endothelial cells [29]. In addition, dextran-Lamp-1 colocalization in SH-SY5Y cells (used in this study) was~80% over 5 h (data not shown). We selected dextran instead of anti-Lamp-1 for our experiments to avoid cell permeabilization which may wash off internalized carriers, and to avoid false-positive cross-detection of anti-ICAM on the carrier coat.

Cells were then incubated with green Fluoresbrite® anti-ICAM NCs for 1 h to ensure sufficient endocytosis, followed by removal of unbound nanocarries and incubation in control medium for 2 or 4 additional hours to allow further intracellular trafficking (total incubation time to track lysosomal transport was 1, 3, or 5 h). Cells were finally fixed with cold 2% paraformaldehyde for 15 min, stained with DAPI to visualized nuclei, and imaged by fluorescence microscopy to calculate the percentage of green fluorescent carriers co-localizing with red dextran-labeled lysosomes, as described [20, 29]. The absolute number of anti-ICAM NCs located within lysosomes in neurites vs. lysosomes in the cell body was also quantified.

Delivery of Enzymes to Lysosomes by ICAM-1-Targeted Nanocarriers

Lysosomes of TNFα-activated SH-SY5Y cells were loaded with Texas-Red dextran as described above, while control cells were not exposed to dextran. Cells were then incubated for 5 h with cell medium containing anti-ICAM NCs co-coated with the enzyme dextranase (anti-ICAM/Dxase NCs). Anti-ICAM NCs void of enzyme served as controls. Along with incubation of carriers, 300 μM chloroquine was added to the samples to avoid lysosomal acidification. This is required to enable Dxase activity while inhibiting activity of lysosomal enzymes, to eliminate any potential contribution of endogenous enzymes of these cells. Cells were finally washed,

fixed and visualized by fluorescence microscopy to quantify the sum intensity of dextran for the whole cell vs. the cell body or neurites.

Statistics

Data were calculated as mean ± standard error of the mean (SEM) from at least four coverslips. Statistical significance was determined as $p < 0.05$ by Student's t-test.

RESULTS

ICAM-1 Expression on Cell Cultures Modeling Control vs. Altered Human Neurons

Since ICAM-1 is known to be expressed on neurons, particularly under inflammation [30], we first verified this with regard to SH-SY5Y cells used in this study. Indeed, immunofluorescence microscopy (Fig. 1a) showed a relatively low baseline level of total ICAM-1 expression on non-stimulated cells (3.3-fold over IgG; not shown). However, as expected (Fig. 1a), ICAM-1 expression significantly increased upon activation with TNFα (known to simulate ICAM-1 overexpression under pathologies underlined with an inflammatory phenotype), rendering ~9.3-fold increased detection over IgG (not shown).

Interestingly, both ICAM-1 expression and its response to stimulation seemed to differentially associate to distinct cellular compartments. For instance, control cells expressed greater levels of ICAM-1 on the cell body vs. neurites, both as total expression (1.9-fold difference) or normalized to the surface area of these two regions (2.4-fold difference; Fig. 1b and c). Under altered conditions (TNFα), total ICAM-1 expression remained higher for the cell body vs. neurites, although the difference was less prominent (1.3-fold difference; Fig. 1b). This resulted from the fact that stimulation of ICAM-1 expression under disease-like conditions was greater on neurites (3.4-fold over control) vs. the cell body (2.3-fold over control). These results suggest potential for drug delivery to neurons via ICAM-1-targeting and validate the adequacy of the cell model used to further explore this strategy.

Binding of ICAM-1-Targeted Nanocarriers to Cell Cultures Modeling Control vs. Diseased Human Neurons

We then assessed the feasibility of targeting ICAM-1 expressed on human neurons. As a model for a polymer nanocarrier, we used green Fluoresbrite®-polystyrene nanoparticles coated with anti-ICAM (anti-ICAM NCs) or control non-specific IgG (IgG NCs). Since polystyrene is not biodegradable, this model allows carrier tracking of targeting and

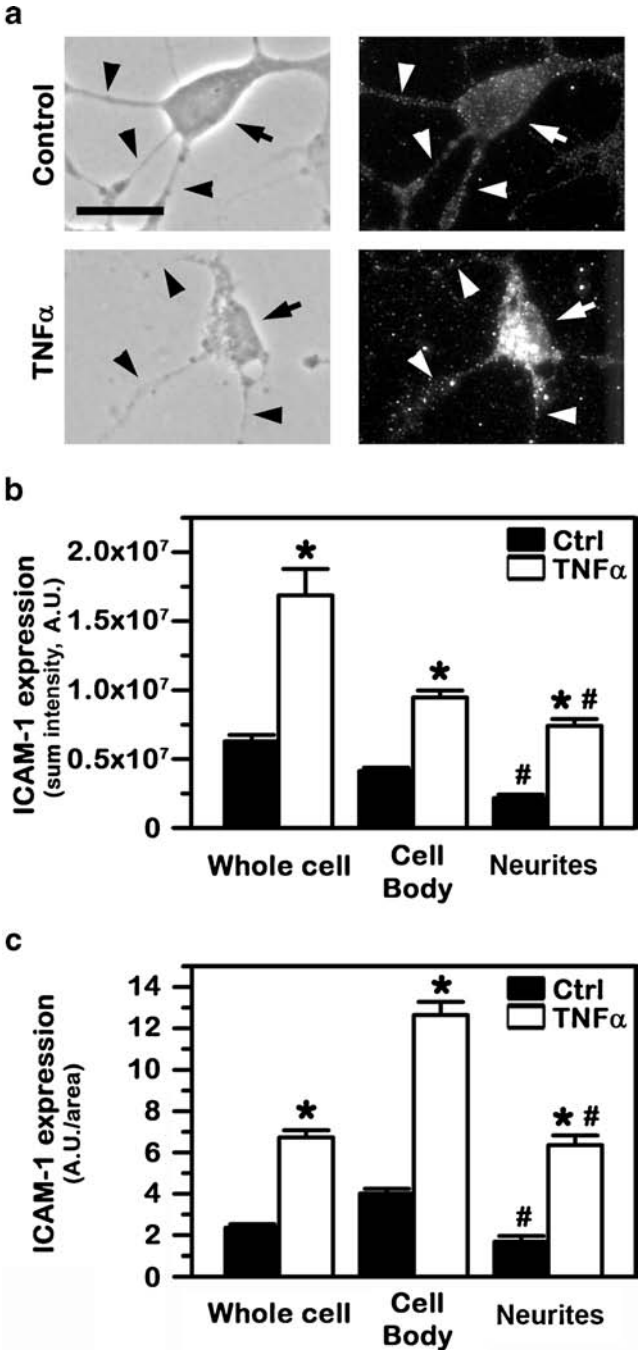

Fig. 1 Comparative expression of ICAM-1 on cell cultures modeling control vs. diseased human neurons. Control vs. TNFα-activated SH-SY5Y cells were fixed and ICAM-1 expressed on the cell surface was detected using anti-ICAM followed by a fluorescence-labeled secondary antibody. (**a**) Phase-contrast showing the cell morphology (left panels) and the corresponding fluorescence imaging showing ICAM-1 expression (right panels). Arrows point to cell bodies, while arrowheads point to cellular processes (neurites). Scale bar = 10 μm. (**b**) Total ICAM-1 expression level, shown as the sum intensity of fluorescence per cell (after subtracting background fluorescence). (**c**) ICAM-1 expression density, shown as the ratio of fluorescence intensity per surface area. Both (**b**) and (**c**) are shown for the whole cell vs. the cell body or neurites. Data are mean ± SEM. *Compares control vs. TNFα within each group; #compares the cell body vs. neurites.

transport (the focus of this study) without potential confounding effects of concomitant carrier degradation. The preparations had a size of 156±2 nm, PDI 0.18±0.01, ζ-potential −27±2 mV, and 227±9 antibodies/carrier for anti-ICAM NCs, and a size of 158±5 nm, PDI 0.19±0.03, ζ-potential −31±2 mV, and 176±8 antibodies/carrier for IgG NCs. These formulations are relatively stable (lack of particle aggregation, antibody detachment, and albumin coating [19, 20]) and render binding, endocytosis, intracellular trafficking, and *in vivo* biodistribution comparable to biocompatible poly(lactic-co-glycolic acid) (PLGA) nanocarriers [31], which validates this model.

While non-specific IgG NCs did not bind to cells under either control or disease-like conditions (5.3±0.7 and 2.6±0.4 NCs/cell; not shown), anti-ICAM NCs did bind under both conditions (5.1-fold and 40.9-fold over IgG NCs, respectively). Also, in agreement with different expression levels of ICAM-1 under these conditions, binding was greater (4-fold) upon TNFα stimulation: 107.5±9.8 NCs/activated cell vs. 27.1±1.8 NCs/control cell (Fig. 2a and b). However, contrary to the higher level of total ICAM-1 expression on the cell body vs. neurites in control conditions, anti-ICAM NCs bound more prominently to the latter region. In each control cell, 18.3±0.8 anti-ICAM NCs bound to neurites vs. 8.8±0.8 NCs bound to the cell body (Fig. 2b). This represents a 2.1-fold difference in binding when normalized to the relative surface area of these two distinct regions (Fig. 2c). This was also the case in each activated cell, where 73.4±3.1 anti-ICAM NCs bound to neurites vs. 34.1±3.1 NCs to the cell body (Fig. 2a and b), a 1.6-fold difference in binding density (Fig. 2c).

Interestingly, binding of anti-ICAM NCs to the cell body of neurons increased between 1 and 5 h to an absolute level comparable to that of neurites (61.8±5.2 NCs; Fig. 3a). This was not the case for binding to neurites, which remained similar during this period of time (73.4±3.1 NCs by 1 h and 65.6±5.2 NCs by 5 h), suggesting a faster saturation for this cellular region. Indeed, binding to neurites achieved a B_{max} of 63.2 NCs/cell with a fast $t_{1/2}$ of less than 1 min, while binding to the neuronal cell body had a B_{max} of 70.2 NCs/cell with a slower $t_{1/2}$ of 83.9 min (not shown). In all cases, saturation was ~40–45 NCs/μm^2 when the relative surface area of these cell compartments was taken into account (Fig. 3b).

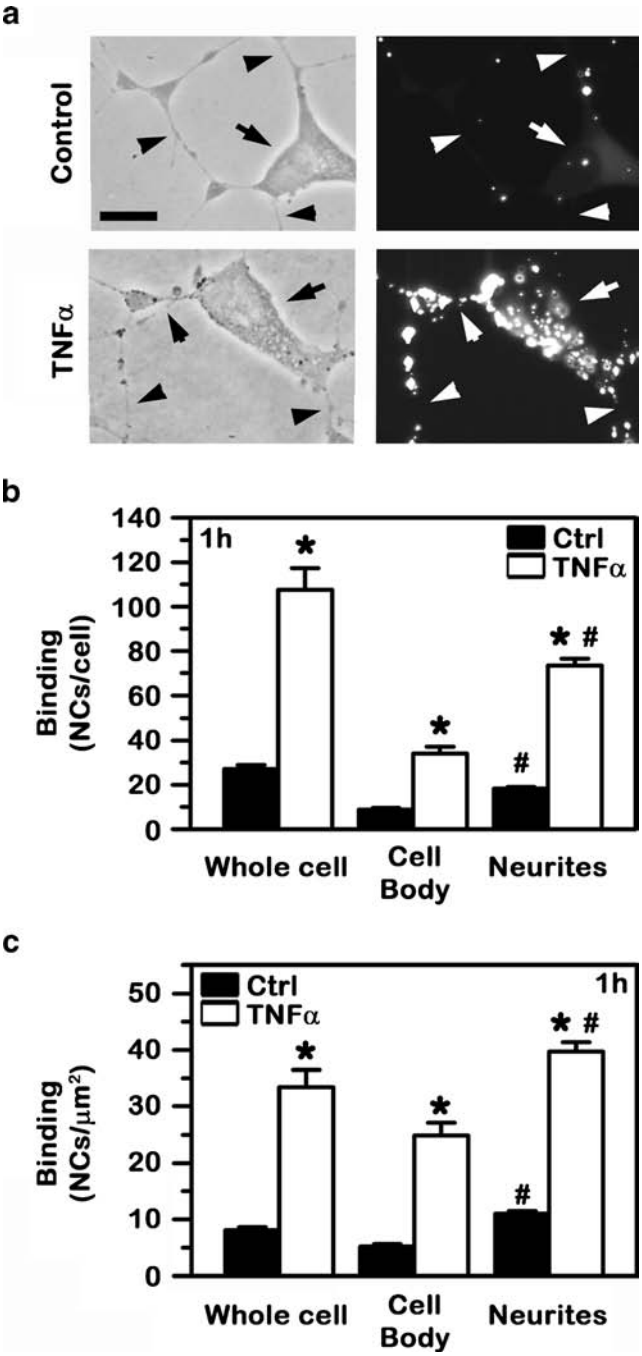

Fig. 2 Binding of anti-ICAM NCs to cell cultures modeling control vs. diseased human neurons. Control vs. TNFα-activated SH-SY5Y cells were incubated with green Fluoresbrite anti-ICAM NCs. Non-bound carriers were then removed, and cells were fixed and imaged by fluorescence microscopy. (**a**) Phase-contrast (left panels) and the corresponding fluorescence images (right panels) are shown. Arrows point to cell bodies, while arrowheads point to neurites. Scale bar = 10 μm. (**b**) The total number of nanocarriers associated to the whole cell vs. the cell body or neurites and (**c**) the number of nanocarriers normalized to the corresponding surface area of these regions are shown. Data are mean ± SEM. *Compares control vs. TNFα; #compares the cell body vs. neurites.

Internalization of ICAM-1-Targeted Nanocarriers by Model Human Neurons

Since internalization within cells is paramount for intracellular delivery, we then assessed this parameter. Lack of significant binding to differentiated SH-SY5Y cells observed above for non-specific IgG NCs precluded tracking of internalization for these control carriers. In contrast, in agreement with their specific binding, uptake of anti-ICAM NCs by this model of human neurons was measureable under both control and altered conditions, with greater uptake for the latter case:

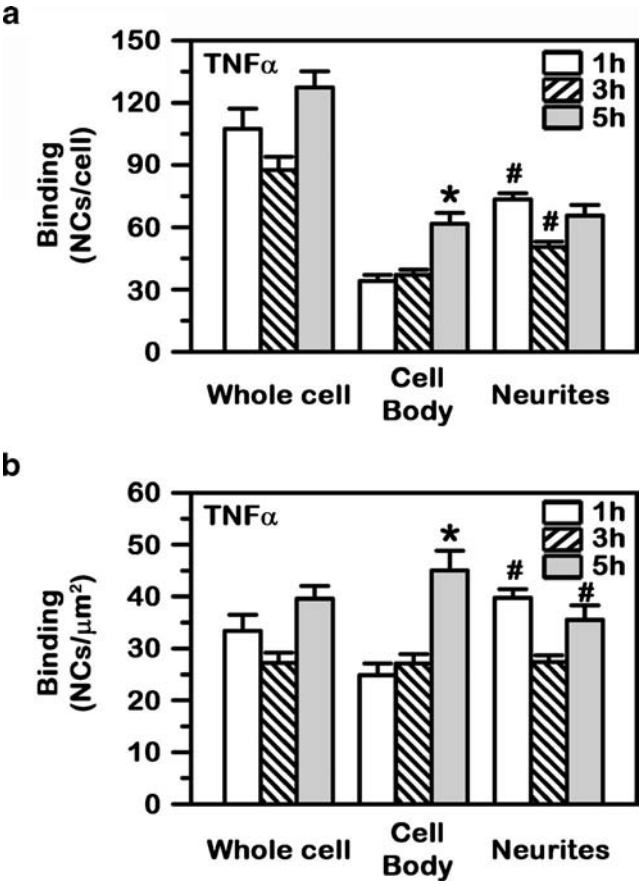

Fig. 3 Differential binding kinetics of anti-ICAM NCs to model human neurons. Binding of green Fluoresbrite anti-ICAM NCs to TNFα-activated SH-SY5Y cells was assessed at 1, 3 and 5 h, as in Fig. 2. (**a**) The total number of nanocarriers associated to the whole cell vs. the cell body or neurites and (**b**) the number of nanocarriers normalized to the corresponding surface area of these regions are shown. Data are mean ± SEM. *Compares 1 vs. 5 h; #compares the cell body vs. neurites.

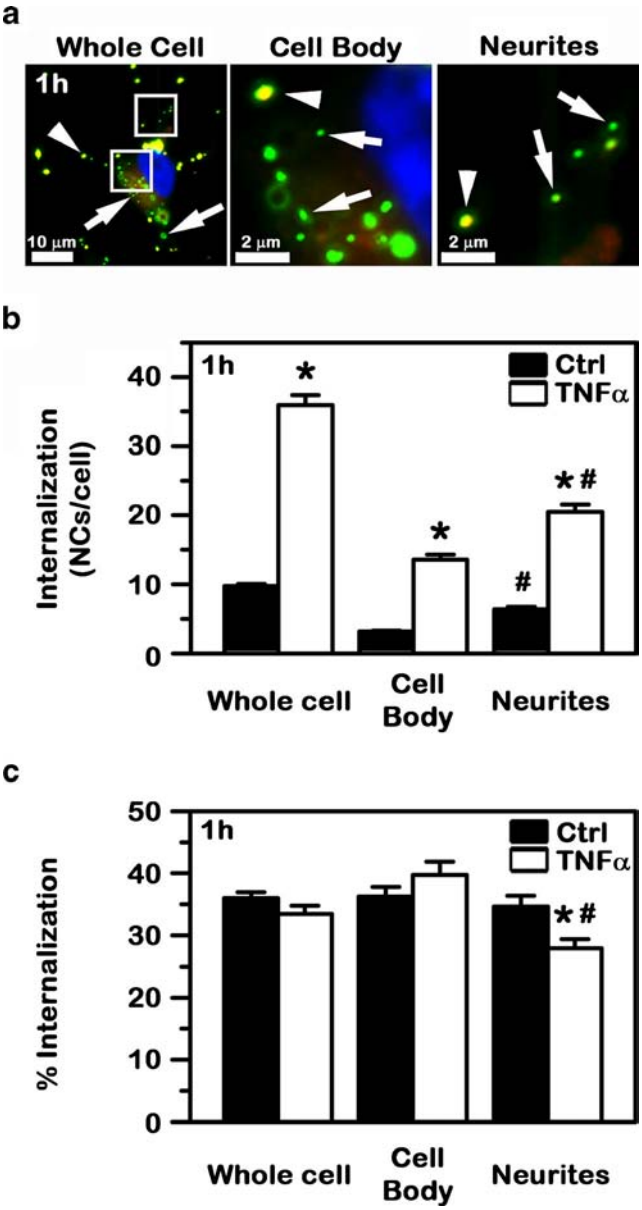

Fig. 4 Internalization of anti-ICAM NCs by cell cultures modeling control vs. diseased human neurons. Control vs. TNFα-activated SH-SY5Y cells were incubated with green Fluoresbrite anti-ICAM NCs. Non-bound carriers were then removed and cells were fixed, followed by differential staining of cell surface-bound, non-internalized carriers with a Texas-Red secondary antibody, and visualization by fluorescence microscopy (see Methods). (**a**) As an example, yellow (green + red) surface-bound carriers (*arrowheads*) vs. green carriers internalized within cells (*arrows*) are shown in TNFα-activated cells. Scale bar = 10 or 2 μm, as specified. (**b**) The absolute number of carriers internalized and (**c**) the percentage of internalized carriers relative to the total number of cell-associated carriers are shown. Data are mean ± SEM. *Compares control vs. TNFα; #compares the cell body vs. neurites.

9.7 ± 0.3 and 35.9 ± 1.4 NCs internalized/cell by 1 h, respectively (Fig. 4a and b). With regard to the percentage of uptake relative to the total amount of carriers associated to cells (Fig. 4c), which reflects the rate or efficacy of the internalization process, this was modestly efficient (~35% at 1 h) and similar for both control and TNFα-treated cells. This suggests that the cell pathophysiological state does not have an effect on the efficacy of this process and, hence, the absolute internalization rather depends on the level of initial binding.

With regard to differences in neuronal compartments, the absolute number of internalized carriers was greater for disease vs. control conditions in both the cell body and neurites (4.3- and 3.2-fold increase, respectively). Under both control and disease conditions, uptake was higher for neurites vs. the cell body: for each control cell, 6.3 ± 0.3 NCs were internalized in neurites vs. 3.2 ± 0.1 NCs internalized in the cell body, and for each diseased cell, 20.5 ± 1.1 NCs were internalized in neurites vs. 13.6 ± 0.7 NCs in the cell body (Fig. 4a and b). These results are in agreement with the extent of carrier binding observed in these areas (Fig. 3a and b). As per the efficacy (%) of internalization of anti-ICAM NCs, this was similar in both the cell body (36.3 ± 1.6%) vs. neurites (34.6 ± 1.8%; Fig. 4c) in control conditions, but significantly different when cells were stimulated (39.7 ± 2.2% for the cell body vs. 27.9 ± 1.5% for neurites).

In disease-like conditions (Fig. 5a and b), internalization of anti-ICAM NCs by model human neurons had an apparent saturation of 35.7 NCs/cell with a $t_{1/2}$ of 1.2 min. Internalization was slower in the cell body vs. cellular neurites ($t_{1/2}$= 210.1 min vs. less than 1 min), yet it reached a higher saturation level at the former region (i.e. I_{max} of 44.4 NCs/cell or 32.4 NCs/μm^2 vs. 17.3 NCs/cell or 9.3 NCs/μm^2, respectively). Since at saturation the maximal binding of anti-ICAM NCs in the cell body was similar to that of neurites, yet the maximal number of internalized carriers was greater, this suggests that a fraction of carriers associated with neurites may traffic to the cell body over time. Supporting this, when cell-associated carriers were tracked after washing off non-bound carriers from the milieu (to avoid further binding that may confound results; Fig. 5c), we observed that the fraction of internalized NCs decreased in neurites over time (from 65 to 50%), while it increased in the cell body (from 35 to 50%).

Mechanism of Uptake of ICAM-1-Targeted Nanocarriers by Model Human Neurons

In other cell types (including brain endothelium, pericytes, and astrocytes of the BBB), ICAM-1 mediates uptake of ICAM-1-targeted nanocarriers via CAM-mediated endocytosis, which differs from classical clathrin- and caveolae-mediated pathways [21, 24, 25]. Hence, we determined next whether this was the case for model human neurons. As shown in Fig. 6, neither filipin nor MDC (inhibitors of caveolae- and clathrin-mediated endocytosis) affected uptake of anti-ICAM NCs in TNFα-treated differentiated SH-SY5Y cells, while uptake was affected (although only slightly) by amiloride (~16% decrease), suggesting a role for CAM endocytosis.

Interestingly, with regard to neuronal compartments, amiloride affected uptake of anti-ICAM NCs more profoundly at the cell body (~40% reduction), while it had no significant effect at the neurites (~97% of control cells). Treatment with MDC slightly increased uptake of anti-ICAM NCs at neurites (~8% increase; not significant), while also slightly decreasing uptake at the cell body (~88% of control cells; not significant). Filipin did not affect uptake at either cellular region (~95% of control for both cell body and neurites), suggesting lack of caveolae involvement in uptake of anti-ICAM NCs.

Lysosomal Trafficking of ICAM-1-Targeted Nanocarriers in Model Human Neurons

In polarized cells separating distinct body compartments (e.g., brain endothelial or gastrointestinal epithelial cells) anti-ICAM NCs can be transported via transcytosis across the cell body [19, 26]. However, transcytosis is not typically used by non-barrier cells within tissues and the most common intracellular destination of anti-ICAM NCs in such cells is endosomal-lysosomal compartments, as for most other drug delivery formulations [19, 20, 29]. Therefore, we examined lysosomal transport of anti-ICAM NCs in differentiated SH-SY5Y cells.

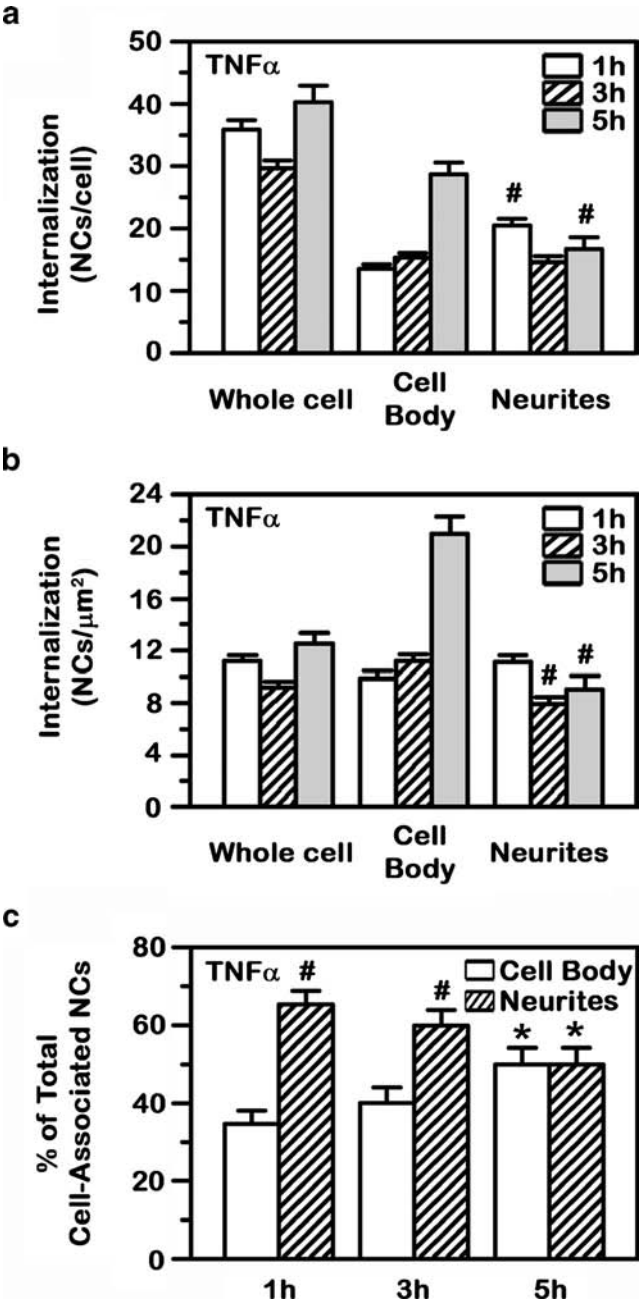

Fig. 5 Comparative internalization kinetics of anti-ICAM NCs by model human neurons. The internalization of green Fluoresbrite anti-ICAM NCs by TNFα-activated SH-SY5Y cells was assessed at the indicated times, as in Fig. 4. (**a**) The absolute number of carriers internalized and (**b**) the number of nanocarriers internalized per surface area are shown. (**c**) Carriers were removed from the milieu after the first hour of incubation (to avoid confounding results of carriers concomitantly binding and being internalized), and cell-associated carriers were then tracked by fluorescence microscopy. The fraction of anti-ICAM NCs located in the cell body vs. neurites is shown. Data are mean ± SEM. #Compares the cell body vs. neurites at each time point (**a-c**); *compares 1 vs. 5 h (**c**).

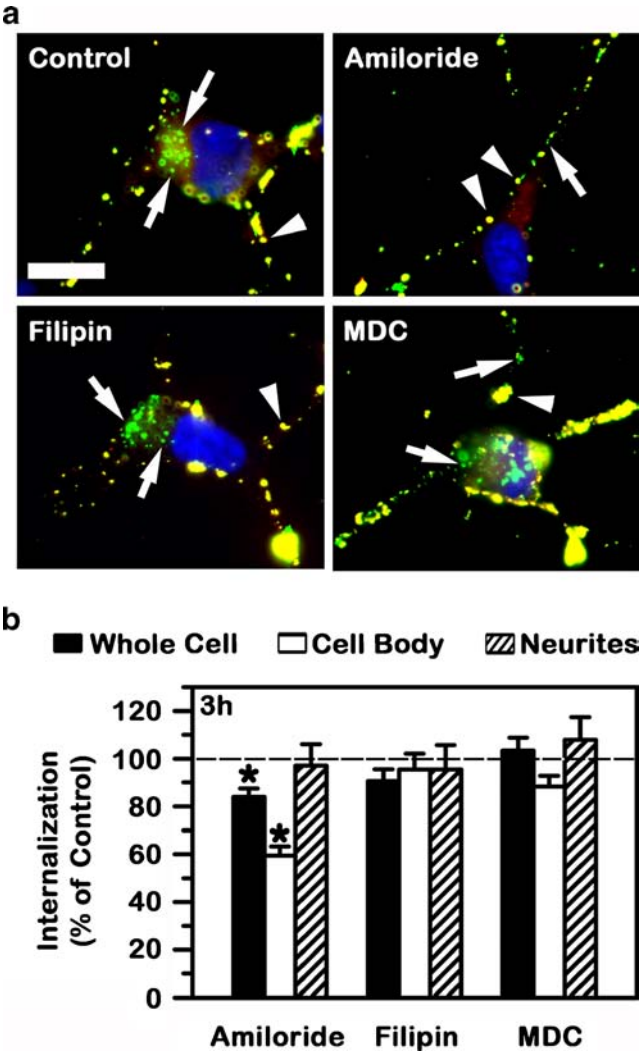

Fig. 6 Endocytic mechanism involved in the uptake of anti-ICAM NCs by model human neurons. The internalization of green Fluoresbrite anti-ICAM NCs by TNFα-activated SH-SY5Y cells was assessed as in Fig. 4, after 3 h incubation in control cell medium or medium containing amiloride, filipin, or monodansylcadaverine (MDC), which inhibit CAM-, clathrin-, or caveolae-mediated endocytosis, respectively. (**a**) Micrographs show yellow surface-bound carriers (*arrowheads*) vs. green internalized carriers (*arrows*). Scale bar = 10 μm. (**b**) The percentage of internalization relative to cells incubated in the absence of inhibitors (control) is shown for the whole cell vs. the cell body or neurites. Data is mean ± SEM. *Compares control vs. inhibitor.

To avoid confounding results of binding and endocytosis concomitant to lysosomal transport, binding and uptake of anti-ICAM NCs was allowed for 1 h (pulse), followed by removal of carriers not associated with cells and tracking of only cell-associated carriers (chase; see Methods). As shown in Fig. 7, anti-ICAM NCs showed a low level of colocalization with intracellular lysosomes in activated neurons by 1 h, but this increased with time, up to ~43% of all cell-associated carriers localizing within this compartment by 3 h (arrows pointing to yellow particles). This seemed to be a saturating level of lysosomal transport, as it did not further increase by 5 h (~46% colocalization), which is in agreement with the total level of ~33% of carriers internalized by this time (Fig. 5). Therefore, focusing only on those carriers internalized by cells, the level of lysosomal transport would be~100%.

With regard to differences in neuronal compartments, anti-ICAM NCs seemed to traffic differently to lysosomes within the cell body as compared to neurites: ~55 and ~37%, respectively, for 5 h (Fig. 7b). The quicker trafficking pattern within the cell body vs. neurites was already seen by 1 h: ~42 vs. ~20% colocalization, respectively. This indicates that lysosomal transport was relatively fast after endocytosis in both regions, particularly in the cell body ($t_{1/2}$ of 22.2 vs. 75.9 min and T_{max} of 57.2 vs. 47.9% in the cell body vs. neurites, respectively).

Since this set of experiments was performed in a pulse-chase mode (see above), the total number of anti-ICAM NCs associated to cells remained constant over time (~85 NCs/cell). As such, we were able to infer potential movement of carriers between neurites and the cell body during said transport. As shown in Fig. 7c, the number of anti-ICAM NCs in lysosomes within neurites decreased between 3 and 5 h (from 26 to 18 NCs), while anti-ICAM NCs in lysosomes within the cell body slightly increased (from 18 to 22 NCs), suggesting carrier transport from the former to the latter compartments.

Therapeutic Effects of Lysosomal Delivery of a Model Enzyme by ICAM-1-Targeted Nanocarriers in Human Neurons

Effective transport of anti-ICAM NCs to lysosomes in differentiated SH-SY5Y cells suggest that potential therapeutic applications of ICAM-1-targeting in neurons will require carriers capable of endo-lysosomal escape to allow delivery to other subcellular destinations, or drugs capable of diffusion from this compartment into the cytosol upon lysosomal degradation of carriers [27]. In addition, such lysosomal routing is ideal for lysosomal delivery of therapeutics whose action is required precisely at this subcellular destination. This is the case for the lysosomal storage disorders (LSDs), a group of about 50 different diseases, most of which associate with fatal dysfunctions affecting most body organs, including the brain [6]. LSDs are due to genetic deficiencies affecting the activity of lysosomal enzymes, leading to lysosomal accumulation of aberrant amounts of undegraded metabolites [6]. Hence, efficient neuronal endocytosis followed by lysosomal transport of enzymes administered exogenously is paramount to developing enzyme replacement therapies for these conditions.

We examined whether anti-ICAM NCs can deliver enzymes to lysosomes in human neurons. For this purpose, we used a model consisting of loading lysosomes of differentiated SH-SY5Y cells with Texas Red dextran, a polysaccharide that cannot be degraded by mammalian cells. Dxase (an enzyme that degrades dextran into glucose [32], which is then able to enter into the cytosol via lysosomal glucose transporters [33]) was co-coated on the surface of anti-ICAM NCs in order to

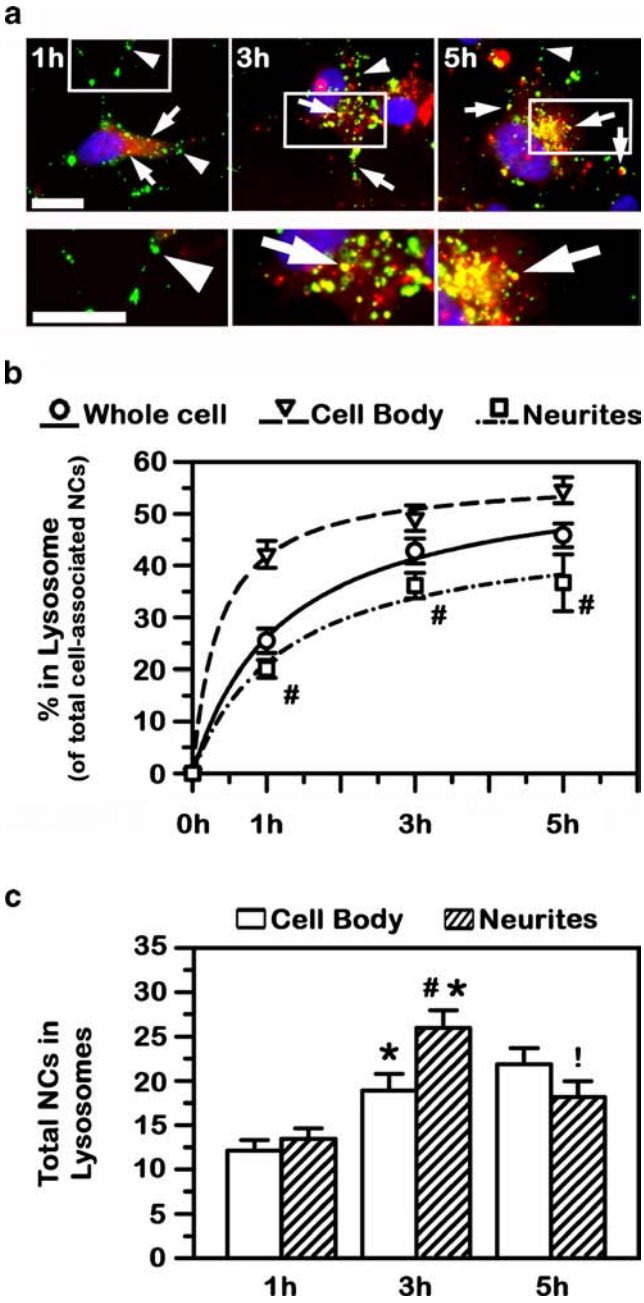

Fig. 7 Lysosomal trafficking of anti-ICAM NCs in model human neurons. Transport of green Fluoresbrite anti-ICAM NCs to Texas-Red dextran-labeled lysosomes in TNFα-activated SH-SY5Y cells was assessed after incubation for 1, 3, or 5 h (see Methods for details). (**a**) Co-localization of green carriers with red lysosomes appears in yellow (*arrows*), while lack of lysosomal co-localization is visualized in green (*arrowheads*). Scale bar = 10 μm. (**b**) The percentage of anti-ICAM NCs co-localizing with lysosomes, relative to the total number of nanocarriers associated with cells, is represented for the whole cell vs. the cell body or neurites. (**c**) The number of anti-ICAM NCs located in lysosomes within the cell body vs. neurites is shown. Data is mean ± SEM. #Compares the cell body vs. neurites at each time point (**b**, **c**); *compares 1 h vs. 3; and !compares 3 vs 5 h (**c**).

explore whether lysosomal delivery of this enzyme would result in dextran degradation. Anti-ICAM/Dxase NCs had a size of 163 ± 4 nm, PDI 0.18 ± 0.02, and ζ-potential −31 ± 1 mV (similar to that of anti-ICAM NCs described above), and carrying 45 nM Dxase. As shown in Fig. 8, incubation of anti-ICAM/Dxase NCs (but not control anti-ICAM NCs) with model human neurons resulted in a significant reduction of dextran accumulated within lysosomes of these cells (~52% reduction in dextran accumulation within 5 h, compared to untreated cells). Degradation was found in both the cell body and neurites, yet somewhat enhanced in the former region (54% in the cell body vs. 47% in neurites; Fig. 8b), which is in agreement with greater lysosomal trafficking in this region. This indicates that Dxase enzyme was successfully transported to lysosomes in differentiated neuroblastoma cells, where it exerted its hydrolytic activity.

DISCUSSION

With a strong effort being paid to improving drug delivery into the CNS (a plethora of helpful strategies are currently under investigation to bypass the BBB [1–6]), understanding how drug delivery platforms interact with the different cell types in the brain is becoming a compelling task. Effective treatment of many neurological conditions requires intracellular drug delivery within neurons [1–6], rendering the study of drug delivery systems necessary in neuronal models. Whether the receptors targeted at the BBB are similarly accessible and functional in neurons, whether they can grant accumulation of therapeutics into these cells despite their ability to cross cells of the BBB, whether pathways (canonical or alternative) that operate in BBB cells are similarly present in neurons, and how interaction of drug carriers with these cells differs relative to the distinct morphological/functional regions found in neurons vs. other cell types (e.g., the cell body vs. neurites) remain open questions. Focusing on the example of ICAM-1-targeted carriers, previously shown to traverse both endothelial and subendothelial elements of the BBB [19], the results described in this study shed light on several aspects of these questions and provide evidence that this strategy holds potential to deliver therapeutic agents into neurons. Whether this pattern applies to carriers targeting different routes of uptake, e.g., the clathrin or caveolar routes, remains unexplored and warrants further investigation.

First, ICAM-1 expression on model human neurons, particularly in disease-like conditions, confirmed expectations based on the literature [30]. Yet, levels of expression and response to disease conditions were different in distinct neuronal compartments: greater ICAM-1 expression was observed for the cell body vs. neurites (Fig. 9a), yet upregulation of expression upon TNFα treatment (which mimics ICAM-1 overexpression under pathological stimulation) was slightly greater on the latter compartment. A priori, different ICAM-1 expression suggests that by tailoring the avidity of

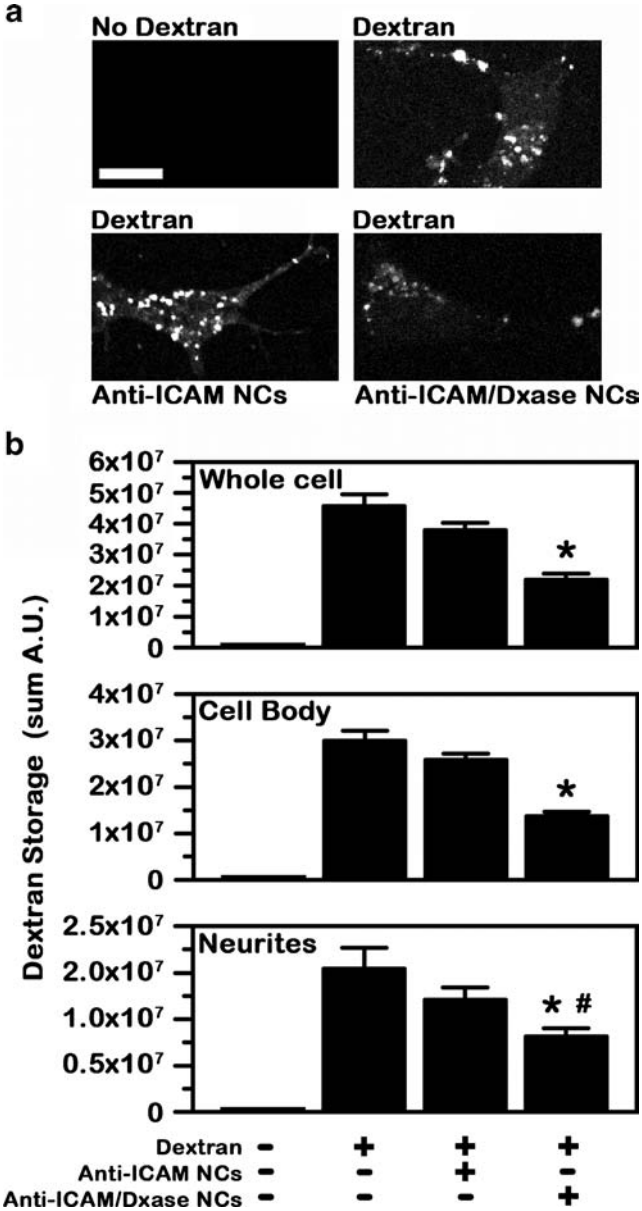

Fig. 8 Effects of lysosomal delivery of a model enzyme by anti-ICAM NCs in model human neurons. Degradation of Texas-Red dextran in lysosomes of TNFα-activated SH-SY5Y cells by dextranase delivered by anti-ICAM NCs (anti-ICAM/Dxase NCs). Anti-ICAM NCs void of enzyme were used as control. Carriers were incubated with cells for 5 h in the presence of 300 μM chloroquine, to avoid lysosomal acidification required for Dxase activity. (**a**) Fluorescence images show the level of accumulation of Texas-Red dextran in cells incubated without vs. with dextran and in the absence or presence of anti-ICAM NCs or anti-ICAM/Dxase NCs. Scale bar = 10 μm. (**b**) Texas-Red dextran sum intensity. Data is mean ± SEM. *Compares nanocarrier-treated cells vs. untreated cells; $^{\#}$compares the cell body vs. cellular neurites.

carriers to be low (or high), neurites may be precluded from (or included in) being targeted, which also depends on the particular status of the tissue. Hence, this knowledge offers an opportunity for modulation of the properties of the system and will guide selection of the particular therapeutic applications where these features may be an asset. This result was unexpected and likely related to specific subcellular functions, and highlights the importance of studying aspects of drug delivery with subcellular distinction when focusing on neurons vs. cells whose body is more uniform in morphology.

Surprisingly, the extent of nanocarrier binding to ICAM-1 on neurons did not completely correspond with the relative level of ICAM-1 expression. As expected, anti-ICAM NC binding was increased under disease conditions in a similar manner as in the case of ICAM-1 expression (4-fold and 3-fold in the whole cell, respectively), which is a desirable feature for drug delivery. However, while the total expression was greater on the cell body vs. neurites, greater binding of anti-ICAM NCs to neurites was achieved (Fig. 9a). A speculation is that this may result from ICAM-1 being differently displayed or positioned on these two neuronal compartments, or the possibility that ICAM-1 may be differentially engaged in interactions with other molecules in these regions, perhaps affecting carrier binding avidity. As a result, it is possible that ICAM-1 expressed on both subcellular locations may be similarly accessible to antibodies in solution (used to label ICAM-1 expression on the cell surface) since they are relatively small. Yet, anti-ICAM on the coat of nanocarriers represents a much bulkier ligand, which may not be able to similarly access the receptor expressed on these two regions due to differential steric hindrances. Whichever the reason, this result indicates that expression of a selected receptor on the cell surface does not necessarily grant access to targeted nanocarriers and this may depend on the particular region of the cell being addressed. Although similar results on different accessibility of antibodies vs. antibody-coated nanocarriers have been previously described in other cases [34], this is the first time that such phenomenon is detected with regard to subcellular regions on a cell.

Once more, this highlights the relevance of studying the interaction of drug delivery systems with neurons at a subcellular scale. For instance, the apparent greater binding of anti-ICAM NCs on neurites vs. the cell body of neurons seemed to pair well with faster binding kinetics at the former region (Fig. 9a). This may be advantageous for delivery of agents which may be required to first interact with neuronal processes, such as axons or dendrites. Given this, perhaps ICAM-1 would provide differential targeting in white vs. grey regions of the brain and/or along neurons encompassing different brain regions, thus guiding the type of suitable application for such a platform and, hence, our future *in vivo* studies. It is tempting to speculate that the neuronal cell body would be more readily accessible vs. areas of the nervous system where axons are myelinated, and applications should be developed with this in mind. Indeed, as found in this work, the number of carriers associated with the cell body reached (over time) similar saturating levels than those associated with neurites. This could be due to the fact that, although likely more accessible

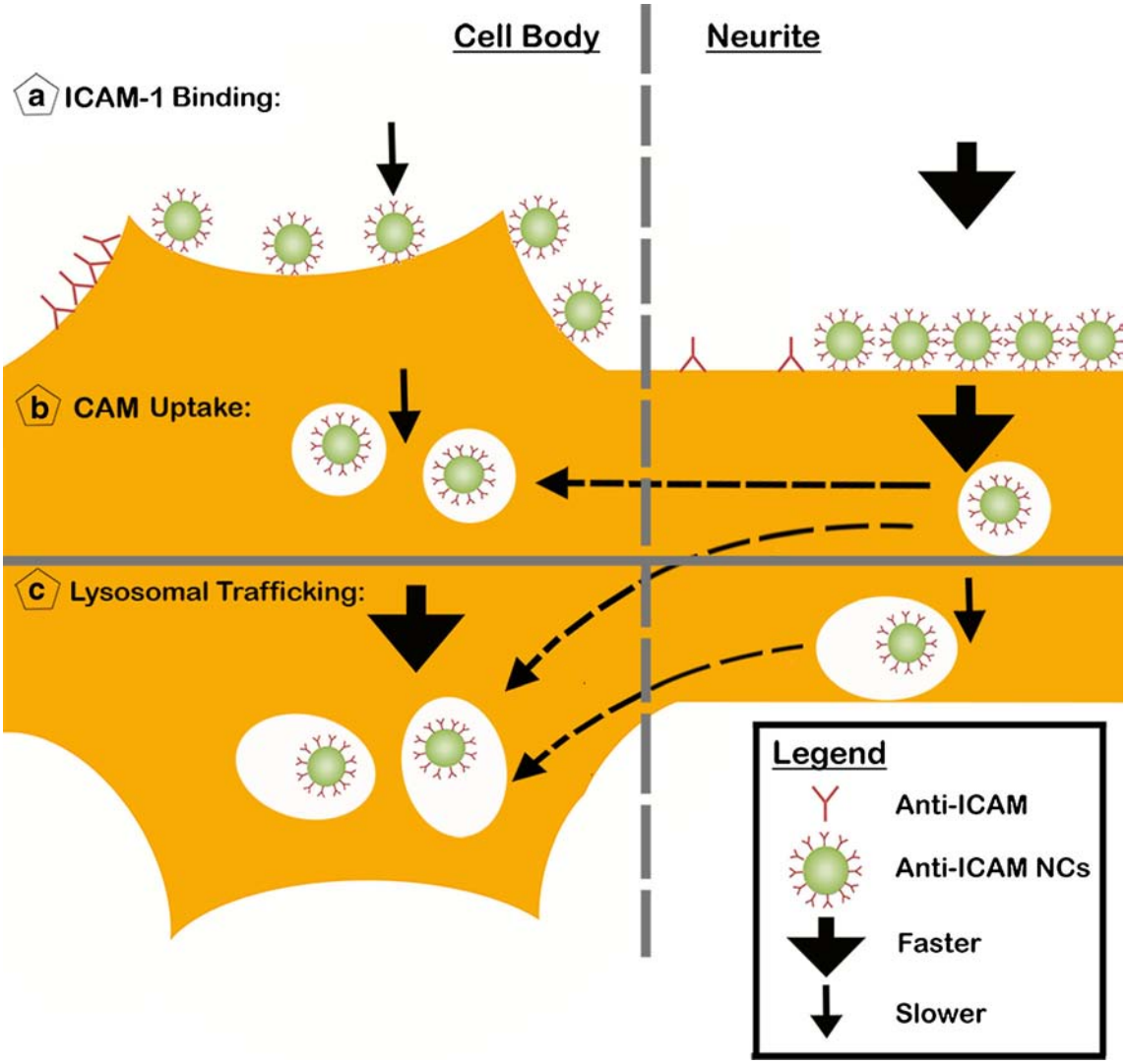

Fig. 9 Schematic representation summarizing the interaction of anti-ICAM NCs with model human neurons. (**a**) Binding of both anti-ICAM and anti-ICAM NCs to model human neurons (SH-SY5Y cells). For each formulation, the relative level of binding per cell compartment (cell body vs. neurites) and their binding density (per surface area, represented as distance) are shown. (**b**) Differential endocytosis of anti-ICAM NCs in neurites vs. the cell body and (**c**) differential trafficking to lysosomes in each compartment. The total number of anti-ICAM NCs shown to be bound (**a**), internalized (**b**), and within lysosomes (**c**) is relative to their level at the saturation time for each of these events at each compartment (cell body vs. neurites). The thickness of arrows shown is relative to the kinetics of anti-ICAM NC binding (**a**), uptake (**b**), and lysosomal transport (**c**) comparing between the cell body vs. neurites.

to nanocarriers, ICAM-1 was expressed at lower levels on cellular neurites.

Beyond binding on the cell surface, anti-ICAM NCs were also internalized by neurons, as previously described in other cell types, including endothelial, epithelial, fibroblasts, mesothelioma, and subendothelial elements of the BBB, such as pericytes and astrocytes [19, 20, 23, 26]. The uptake efficacy (reflected by the ratio between the number of nanocarriers internalized vs. total nanocarriers associated to cells) was somewhat lower than that of other cell types: ~33% compared to ~50% internalization efficiency seen in non-endothelial brain cells, specifically astrocytes and pericytes [19]. The absolute number of nanocarriers internalized by model human neurons directly correlated with their level of binding, this being greater for neurites vs. the cell body and enhanced in both areas under disease-like conditions. Similar to the binding pattern, the internalization kinetics was slower for the cell body (Fig. 9b). Yet, different from binding, internalization reached higher saturating levels in this cell region (Fig. 9b). This, along with the fact that the number of anti-ICAM NCs located at neurites decreased over time, with a concomitant increase of anti-ICAM NCs at the cell body, suggests that at least a fraction of anti-ICAM NCs traffic from neurites to the cell body (Fig. 9b), rendering the overall net accumulation greater in this area over time.

As per the endocytic mechanism involved, this was related to the CAM pathway, as previously described in the case of ICAM-1 targeting in other cell types [19, 20, 25, 26]. This is an important finding because the existence of clathrin- and caveolae-independent pathways, although reported for other

cells, is rather unknown in the case of neurons and, therefore, represents a new avenue to explore drug delivery in the brain. This is also relevant since the CAM pathway appears to have less limiting restrictions regarding the geometry of carriers able to internalize via this route vs. the clathrin and caveolar paths [21–24]. Also, a number of neurological diseases associate with impairment of classical caveolae- and clathrin-dependent pathways, rendering suboptimal delivery of drug delivery strategies that capitalize on these routes [6, 35]. Apart from this, other interesting observations were made in neurons. For instance, while the CAM pathway clearly operated at the cell body with regard to uptake of anti-ICAM NCs, clathrin-mediated endocytosis seemed to influence uptake into neurites: inhibition of clathrin-coated pits slightly enhanced uptake of anti-ICAM NCs at this region. An explanation for this effect is that clathrin-mediated endocytosis is known to be highly active in neuronal processes [36] and, hence, a fraction of anti-ICAM NCs bound to the cell surface at these regions may be passively internalized via the clathrin route simple as a consequence of this high activity. However, when clathrin pathways are inhibited, all nanocarriers are endocytosed via the CAM route, which is more efficient toward this ligand due to its specificity and, therefore, results in enhanced uptake under this circumstance. We have recently reported a similar phenomenon in the case of uptake of anti-ICAM NCs by brain endothelial cells [19], perhaps this behavior specifically associates with brain cells with high frequency of endocytic activity. In any case, this highlights that even when targeted to specific pathways and despite the fact that targeted pathways may rule the final outcome, uptake of nanocarriers can still be influenced by parallel routes depending on the basal activity of a specific cell type or tissue.

With regard to intracellular trafficking, we found that anti-ICAM NCs were transported to lysosomes both in neurites and the cell body. This is possible since lysosomes have been reported to exist in both regions of a neuron [37] and endosomes also traffic towards the cell body via retrograde axonal transport [38]. It is important to emphasize that lysosomal transport was observed under disease-like conditions, because a number of neurodegenerative diseases exhibit impaired axonal transport and lysosomal activity, including Alzheimer's disease, Parkinson's disease, and several LSDs [39]. This lysosomal trafficking seemed relatively fast, with faster kinetics in the case of the cell body vs. neurites (Fig. 9c). Curiously, this is opposite the pattern of endocytosis of anti-ICAM NCs within these cells (Fig. 9b), as discussed above, and may be due to some retrograde transport from cellular process toward cell body lysosomes (Fig. 9c). The fact that the number of lysosomal-colocalizing carriers decreased between 3 and 5 h in neurites, while it increased in the cell body, supports this hypothesis.

This transport pattern shall guide future selection of suitable therapeutic applications of ICAM-1-targeting in neurons. For instance, applications which require drug delivery to other subcellular destinations should employ carriers capable of endo-lysosomal escape, such as the case we recently reported where anti-ICAM was coupled to dendrimers built of DNA [27]. These were able to disrupt endosomal compartments with delivery of different cargoes (including toxins, sugars, proteins, and nucleic acids) into the cytosol and nucleus of cells [27]. Other applications may focus on drugs which can diffuse into the cytosol upon lysosomal degradation of carriers or cell penetrating peptides, as in the case for certain anti-inflammatory agents or chemotherapeutics (dexomethasone, doxorubicin, etc.) [40].

Yet, perhaps the most suitable application for intracellular routing of anti-ICAM NCs is that of enzyme replacement therapy for lysosomal dysfunctions, such as the LSDs due to genetic deficiencies of lysosomal enzymes. This leads to aberrant accumulation of undegraded metabolites within lysosomes of most cells in the body (including peripheral tissues and the CNS) [6], hence, requiring broad lysosomal delivery rather than tissue-specific targeting. Indeed, since ICAM-1 is expressed throughout the body, anti-ICAM NCs loaded with lysosomal enzymes have been observed to markedly enhance biodistribution of such therapeutic agents in all organs, including the brain [20, 21]. Along with the fact that ICAM-1 targeting provides transport across endothelial and subendothelial linings of the BBB [19], lysosomal transport of anti-ICAM NCs in neurons (as observed in this study), holds great potential to improve the therapeutic outcome of lysosomal enzyme replacement therapies in this organ, a currently unmet medical need [6]. The model example showed here demonstrated degradation of substrate accumulated within lysosomes upon delivery of an exogenous enzyme via ICAM-1 targeting. This result validates our hypothesis and pairs well with a similar efficacy shown for this platform in other cell types [6, 20, 26].

Overall, ICAM-1 targeting holds considerable potential with regard to intracellular drug delivery in the brain, such as the case of treatment of LSDs with neurological component. Future studies will focus on examining the delivery efficacy and effects of this platform *in vivo* utilizing clinically relevant, biodegradable carriers.

ACKNOWLEDGMENTS AND DISCLOSURES

The authors thank Dr. Estrella Rubio Solsona (Program in Rare and Genetic Diseases & IBV/CSIC Associated Unit, Centro de Investigación Príncipe Felipe, Valencia, Spain) for her guidance in propagating and differentiating SH-SY5Y cells. We also thank Rachel Manthe (Department of Bioengineering, University of Maryland, College Park, MD, USA) for help with grammar edits. This work was supported by NIH grant R01-HL09816 and NSF award CBET-1402756 (S.M.).

REFERENCES

1. Barchet TM, Amiji MM. Challenges and opportunities in CNS delivery of therapeutics for neurodegenerative diseases. Expert Opin Drug Deliv. 2009;6(3):211–25.
2. Abbott NJ. Blood–brain barrier structure and function and the challenges for CNS drug delivery. J Inherit Metab Dis. 2013;36(3): 437–49.
3. Dhuria SV, Hanson LR, Frey WH. 2nd. Intranasal delivery to the central nervous system: mechanisms and experimental considerations. J Pharm Sci. 2010;99(4):1654–73.
4. Lakhal S, Wood MJ. Exosome nanotechnology: an emerging paradigm shift in drug delivery: exploitation of exosome nanovesicles for systemic *in vivo* delivery of RNAi heralds new horizons for drug delivery across biological barriers. BioEssays. 2011;33(10):737–41.
5. Neuwelt E, Abbott NJ, Abrey L, Banks WA, Blakley B, Davis T, *et al.* Strategies to advance translational research into brain barriers. Lancet Neurol. 2008;7(1):84–96.
6. Muro S. Strategies for delivery of therapeutics into the central nervous system for treatment of lysosomal storage disorders. Drug Deliv Transl Res. 2012;2(3):169–86.
7. Hoffman AS. The origins and evolution of "controlled" drug delivery systems. J Control Release. 2008;132(3):153–63.
8. Muro S. Challenges in design and characterization of ligand-targeted drug delivery systems. J Control Release. 2012;164(2):125–37.
9. Albertazzi L, Gherardini L, Brondi M, Sulis Sato S, Bifone A, Pizzorusso T, *et al. In vivo* distribution and toxicity of PAMAM dendrimers in the central nervous system depend on their surface chemistry. Mol Pharm. 2012;10(1):249–60.
10. Boussif O, Lezoualc'h F, Zanta MA, Mergny MD, Scherman D, Demeneix B, *et al.* A versatile vector for gene and oligonucleotide transfer into cells in culture and *in vivo*: polyethylenimine. Proc Natl Acad Sci U S A. 1995;92(1):7297–301.
11. O'Mahony AM, Godinho BM, Ogier J, Devocelle M, Darcy R, Cryan JF, *et al.* Click-modified cyclodextrins as nonviral vectors for neuronal siRNA delivery. ACS Chem Neurosci. 2012;3(10):744–52.
12. Boado RJ, Zhang Y, Wang Y, Pardridge WM. Engineering and expression of a chimeric transferrin receptor monoclonal antibody for blood–brain barrier delivery in the mouse. Biotechnol Bioeng. 2009;102(4):1251–8.
13. LeBowitz JH, Grubb JH, Maga JA, Schmiel DH, Vogler C, Sly WS. Glycosylation-independent targeting enhances enzyme delivery to lysosomes and decreases storage in mucopolysaccharidosis type VII mice. Proc Natl Acad Sci U S A. 2004;101(9):3083–8.
14. Osborn MJ, McElmurry RT, Peacock B, Tolar J, Blazar BR. Targeting of the CNS in MPS-IH using a nonviral transferrin-alpha-L-iduronidase fusion gene product. Mol Ther. 2008;16(8): 1459–66.
15. Budzinski KL, Sgro AE, Fujimoto BS, Gadd JC, Shuart NG, Gonen T, *et al.* Synaptosomes as a platform for loading nanoparticles into synaptic vesicles. ACS Chem Neurosci. 2011;2(5):236–41.
16. Deinhardt K, Berninghausen O, Willison HJ, Hopkins CR, Schiavo G. Tetanus toxin is internalized by a sequential clathrin-dependent mechanism initiated within lipid microdomains and independent of epsin1. J Cell Biol. 2006;174(3):459–71.
17. Francesconi A, Kumari R, Zukin RS. Regulation of group I metabotropic glutamate receptor trafficking and signaling by the caveolar/lipid raft pathway. J Neurosci. 2009;29(11):3590–602.
18. Rothlein R, Springer TA. The requirement for lymphocyte function-associated antigen 1 in homotypic leukocyte adhesion stimulated by phorbol ester. J Exp Med. 1986;163(5):1132–49.
19. Hsu J, Rappaport J, Muro S. Specific binding, uptake, and transport of ICAM-1-targeted nanocarriers across endothelial and subendothelial cell components of the blood–brain barrier. Pharm Res. 2014;31(7):1855–66.
20. Hsu J, Serrano D, Bhowmick T, Kumar K, Shen Y, Kuo YC, *et al.* Enhanced endothelial delivery and biochemical effects of alpha-galactosidase by ICAM-1-targeted nanocarriers for Fabry disease. J Control Release. 2011;149(3):323–31.
21. Papademetriou I, Garnacho C, Serrano D, Bhowmick T, Schuchman EH, Muro S. Comparative binding, endocytosis, and biodistribution of antibodies and antibody-coated carriers for targeted delivery of lysosomal enzymes to ICAM-1 versus transferrin receptor. J Inherit Metab Dis. 2013;36(3):467–77.
22. Ansar M, Serrano D, Papademetriou I, Bhowmick TK, Muro S. Biological functionalization of drug delivery carriers to bypass size restrictions of receptor-mediated endocytosis independently from receptor targeting. ACS Nano. 2013;7(12):10597–611.
23. Muro S, Garnacho C, Champion JA, Leferovich J, Gajewski C, Schuchman EH, *et al.* Control of endothelial targeting and intracellular delivery of therapeutic enzymes by modulating the size and shape of ICAM-1-targeted carriers. Mol Ther. 2008;16(8):1450–8.
24. Serrano D, Bhowmick T, Chadha R, Garnacho C, Muro S. Intercellular adhesion molecule 1 engagement modulates sphingomyelinase and ceramide, supporting uptake of drug carriers by the vascular endothelium. Arterioscler Thromb Vasc Biol. 2012;32(5):1178–85.
25. Muro S, Wiewrodt R, Thomas A, Koniaris L, Albelda SM, Muzykantov VR, *et al.* A novel endocytic pathway induced by clustering endothelial ICAM-1 or PECAM-1. J Cell Sci. 2003;116(Pt 8):1599–609.
26. Ghaffarian R, Bhowmick T, Muro S. Transport of nanocarriers across gastrointestinal epithelial cells by a new transcellular route induced by targeting ICAM-1. J Control Release. 2012;163(1):25–33.
27. Muro S. A DNA device that mediates selective endosomal escape and intracellular delivery of drugs and biologicals. Adv Funct Mater. 2014;24(19):2899–906.
28. Gimenez-Cassina A, Lim F, Diaz-Nido J. Differentiation of a human neuroblastoma into neuron-like cells increases their susceptibility to transduction by herpesviral vectors. J Neurosci Res. 2006;84(4):755–67.
29. Muro S, Cui X, Gajewski CM, Murciano J-C, Muzykantov VR, Koval M. Slow intracellular trafficking of catalase nanoparticles targeted to ICAM-1 protects endothelial cells from oxidative stress. Am J Phys Cell Physiol. 2003;285(5):C1339–47.
30. Birdsall HH. Induction of ICAM-1 on human neural cells and mechanisms of neutrophil-mediated injury. Am J Pathol. 1991;139(6):1341–50.
31. Muro S, Dziubla T, Qiu W, Leferovich J, Cui X, Berk E. Muzykantov VR. Endothelial targeting of high-affinity multivalent polymer nanocarriers directed to intercellular adhesion molecule 1. J Pharmacol Exp Ther. 2006;317(3):1161–9.
32. Khalikova E, Susi P, Korpela T. Microbial dextran-hydrolyzing enzymes: fundamentals and applications. Microbiol Mol Biol Rev. 2005;69(2):306–25.
33. Augustin R, Riley J, Moley KH. GLUT8 contains a [DE] XXXL [LI] sorting motif and localizes to a late endosomal/lysosomal compartment. Traffic. 2005;6:1196–212.
34. Garnacho C, Albelda SM, Muzykantov VR, Muro S. Differential intra-endothelial delivery of polymer nanocarriers targeted to distinct PECAM-1 epitopes. J Control Release. 2008;130(3):226–33.
35. Rappaport J, Garnacho C, Muro S. Clathrin-mediated endocytosis is impaired in type A-B Niemann-Pick disease model cells and can be restored by ICAM-1-mediated enzyme replacement. Mol Pharm. 2014;11(8):2887–95.
36. Blanpied TA, Scott DB, Ehlers MD. Dynamics and regulation of clathrin coats at specialized endocytic zones of dendrites and spines. Neuron. 2002;36(3):435–49.

37. Roberts VJ, Gorenstein C. Examination of the transient distribution of lysosomes in neurons of developing rat brains. Dev Neurosci. 1987;9(4):255–64.
38. Deinhardt K, Salinas S, Verastegui C, Watson R, Worth D, Hanrahan S, *et al.* Rab5 and Rab7 control endocytic sorting along the axonal retrograde transport pathway. Neuron. 2006;52(2):293–305.
39. Millecamps S, Julien JP. Axonal transport deficits and neurodegenerative diseases. Nat Rev Neurosci. 2013;14(3):161–76.
40. Torchilin VP. Recent approaches to intracellular delivery of drugs and DNA and organelle targeting. Annu Rev Biomed Eng. 2006;8:343–75.